



# Poroelastic coefficients for anisotropic single and double porosity media

Qi Zhang<sup>1</sup> · Ronaldo I. Borja<sup>1</sup>

Received: 1 December 2020 / Accepted: 9 March 2021 / Published online: 21 April 2021  
© The Author(s), under exclusive licence to Springer-Verlag GmbH Germany, part of Springer Nature 2021

## Abstract

Closed-form expressions for poroelastic coefficients are derived for anisotropic materials exhibiting single and double porosity. A novel feature of the formulation is the use of the principle of superposition to derive the governing mass conservation equations from which analytical expressions for the Biot tensor and Biot moduli, among others, are derived. For single-porosity media, the mass conservation equation derived from the principle of superposition is shown to be identical to the one derived from continuum principle of thermodynamics, thus confirming the veracity of both formulations and suggesting that this conservation equation can be derived in more than one way. To provide further insight into the theory, numerical values of the poroelastic coefficients are calculated for granite and sandstone that are consistent with the material parameters reported by prominent authors. In this way, modelers are guided on how to determine these coefficients in the event that they use the theory for full-scale modeling and simulations.

**Keywords** Anisotropy · Double porosity · Poroelasticity · Principle of superposition

## 1 Introduction

A large number of existing reservoirs may be categorized as naturally fractured [5, 15, 16, 21, 22, 24–26, 32–34, 44, 45]. By this, we usually refer to materials with distributed discontinuities that they exhibit two very distinct porous networks. Roughly speaking, the first porous network is formed of penny-shaped cracks or fissures mainly due to tectonic activities, while the second is formed of rounded pores [20]. As for their characteristics, the fracture networks are characterized by low storage and high permeability, whereas the porous blocks are characterized by high storage and low permeability [55]. As a result, the behaviors of fractured reservoirs are considerably different from those of conventional reservoirs [25], which could be reflected in the soil consolidation, groundwater flow, solute transport, and gas/oil production [3]. Until now, the modeling of fractured reservoirs is still

one of the most challenging activities in geomechanics and geosciences.

Over the last 50 years, numerous models with different degrees of sophistication have been proposed for porous materials, which can be divided into three categories. In the earliest category, a fractured system was grossly treated as an equivalent single-porosity continuum [40], and the existence of fractures or cracks is reflected in the material coefficients such as stiffness, which may be orders of magnitude different from those of a homogeneous medium [3]. However, this approach has a number of drawbacks such as the identification of the representative blocks and the determination of equivalent permeability values [3, 32]. On the contrary, the second category is known as the explicit (direct) modeling approach such as the discrete fracture network [6, 23, 27, 47], which allows one to account for each length scale directly within a model. However, the very large number of micro-fractures in the unconventional reservoir [37] could make the direct simulation of discrete fracture networks computationally prohibitive [1, 2].

The third category is the double-porosity model [4, 50], which assumed that two pore regions overlap in a computational domain. The main idea is that for every physical

✉ Ronaldo I. Borja  
borja@stanford.edu

<sup>1</sup> Department of Civil and Environmental Engineering,  
Stanford University, Stanford, CA 94305, USA

point in space, there may be two scales of porosity, one representing the average porosity in the fracture network and the other in the porous blocks [20]. This idealization may be thought of as an extreme case of the crack density model of Wong [53] when the micro-fracture density becomes very high. The mathematical basis for this model is known as mixture theory in which any material in a composite medium that is significantly different from those of other intervening materials deserves a separate description. This leads to two mass conservation equations, one for each of the foregoing porosity regions. These equations are coupled by a leakage (source/sink) term [30, 36, 37, 42]. Nowadays, the double-porosity concept has been widely used in civil engineering, energy resource engineering, and many other related fields of engineering [3, 32].

Previous formulations of poroelasticity in double-porosity media have assumed isotropy in both deformation and fluid flow [3, 7, 18, 19, 25, 29, 31, 35, 36, 46, 52, 59]. However, many geologic materials have exhibited anisotropy in either or both deformation and fluid flow responses [14, 28, 41, 43, 49, 54, 57, 60]. In this work, we consider a special case of anisotropy known as transverse isotropy, or cross-anisotropy, which is characterized by a plane on which the response is isotropic and an axis perpendicular to this plane on which the response is anisotropic. For a single-porosity medium, the effect of transverse isotropy has already been incorporated into the poroelasticity equations [17, 49, 58]. For a double-porosity medium, however, its effect has not been clearly elucidated in light of the limitations imposed by current laboratory testing procedures.

The aim of this paper is to address the above-mentioned knowledge gap in the poroelasticity of anisotropic double-porosity media. A novel feature of the mathematical formulation is the use of the principle of superposition in combination with mixture theory to arrive at the governing mass balance equations. The mathematical formulation is innovative because it leads to a result that is identical to what has been developed previously using continuum principles of thermodynamics [58], but following a different route. It is the first time, to the authors' knowledge, that these new formulas and interpretations are presented within the context of poromechanics.

However, we emphasize at the outset that the principle of superposition is applied in this paper at a fixed hydromechanical state where only mechanical deformation is involved, and not from one hydromechanical state to another where dissipative processes would render the principle inapplicable. Furthermore, we restrict the developments to linear elasticity. Nevertheless, even with the assumption of poroelasticity, the parameters or coefficients of a model are usually arbitrarily assumed in the literature, and their fundamental origins were not clearly established.

In this respect, the results of this paper are useful in shedding light onto the physical meaning of the governing conservation equations and the relevant poroelastic coefficients.

The paper is organized as follows. Based on mixture theory, mass conservation equations are first formulated in Sect. 2 for single-porosity media, where the evolution laws for the volume fractions are derived. To this end, we make use of the principle of superposition for anisotropic single-porosity media to obtain the poroelastic coefficients and compare them with those derived in [17, 58]. In Sect. 3, we extend the formulation to anisotropic double-porosity media and derive the corresponding poroelastic coefficients analytically. The elastic moduli for transversely isotropic materials are discussed in Sect. 4, where the relevant poroelastic coefficients for two types of rock are also calculated and compared with those derived by prominent authors [8, 29]. Finally, conclusions are given in Sect. 5.

## 2 Single-porosity media

In the following discussion and throughout this paper, we assume that the solid deformation is infinitesimal in the sense that the domain of the problem does not change appreciably. We denote by  $V$  a representative elementary volume (REV) consisting of a mixture of solid and fluid. Let  $\phi^s$  and  $\phi^f$  represent the volume fractions of solid and fluid, respectively, defined as

$$\phi^s = \frac{V_s}{V}, \quad \phi^f = \frac{V_f}{V}, \quad (1)$$

where  $V_s$  and  $V_f$  are volumes of solid and fluid in  $V$ , respectively. The closure condition on the volume fractions is

$$\phi^s + \phi^f = 1. \quad (2)$$

The partial mass densities of the solid and fluid are given by

$$\rho^s = \phi^s \rho_s, \quad \rho^f = \phi^f \rho_f, \quad (3)$$

where  $\rho_s$  and  $\rho_f$  are the intrinsic mass densities of solid and fluid, respectively. The total mass density of the mixture is given by the sum

$$\rho = \rho^s + \rho^f. \quad (4)$$

We denote the material time derivatives following the motions of solid and fluid by  $d(\cdot)/dt$  and  $d^f(\cdot)/dt$ , respectively. The mass balance equations for solid and fluid, assuming no mass exchanges between them, take the form

$$\frac{d\rho^s}{dt} + \rho^s \nabla \cdot \mathbf{v} = 0, \quad (5)$$

$$\frac{d^f \rho^f}{dt} + \rho^f \nabla \cdot \mathbf{v}_f = 0, \quad (6)$$

where  $\mathbf{v}$  and  $\mathbf{v}_f$  are the intrinsic velocities of solid and fluid particles, respectively. Written in terms of  $\rho_s$  and  $\rho_f$ , the conservation equations take the form

$$\frac{d\phi^s}{dt} + \frac{\phi^s}{\rho_s} \frac{d\rho_s}{dt} + \phi^s \nabla \cdot \mathbf{v} = 0, \quad (7)$$

$$\frac{d^f \phi^f}{dt} + \frac{\phi^f}{\rho_f} \frac{d\rho_f}{dt} + \phi^f \nabla \cdot \mathbf{v}_f = 0. \quad (8)$$

Assuming barotropic flow, the constitutive equation relating density and pressure in the solid is given by

$$\frac{1}{\rho_s} \frac{d\rho_s}{dt} = \frac{1}{K_s} \frac{dp_s}{dt}, \quad (9)$$

where  $p_s$  and  $K_s$  are the intrinsic pressure and bulk modulus in the solid. Substituting in Eq. (7) yields

$$\frac{d\phi^s}{dt} + \frac{\phi^s}{K_s} \frac{dp_s}{dt} + \phi^s \nabla \cdot \mathbf{v} = 0. \quad (10)$$

For the fluid, we take a similar intrinsic constitutive relation of the form

$$\frac{1}{\rho_f} \frac{d^f \rho_f}{dt} = \frac{1}{K_f} \frac{d^f p}{dt}, \quad (11)$$

where  $p = p_f$  is the intrinsic pressure in the fluid. Substituting into Eq. (8) gives

$$\frac{d^f \phi^f}{dt} + \frac{\phi^f}{K_f} \frac{d^f p}{dt} + \phi^f \nabla \cdot \mathbf{v}_f = 0. \quad (12)$$

We recall that the material time derivative following the fluid motion is related to the material time derivative following the solid motion through the equation

$$\frac{d^f(\cdot)}{dt} = \frac{d(\cdot)}{dt} + \nabla(\cdot) \cdot \tilde{\mathbf{v}}_f, \quad (13)$$

where  $\tilde{\mathbf{v}}_f = \mathbf{v}_f - \mathbf{v}$  is the relative velocity of fluid with respect to solid. Thus, for the fluid we obtain

$$\frac{d\phi^f}{dt} + \frac{\phi^f}{K_f} \frac{dp}{dt} + \frac{1}{K_f} (\nabla p) \cdot \mathbf{q} + \nabla \cdot \mathbf{q} + \phi^f \nabla \cdot \mathbf{v} = 0, \quad (14)$$

where

$$\mathbf{q} = \phi^f \tilde{\mathbf{v}}_f \quad (15)$$

is the superficial Darcy velocity.

The total Cauchy stress tensor  $\boldsymbol{\sigma}$  may be written as the sum of partial stress tensors in the form

$$\boldsymbol{\sigma} = \phi^s \boldsymbol{\sigma}_s - \phi^f p \mathbf{1}, \quad (16)$$

where  $\boldsymbol{\sigma}_s$  is the intrinsic stress in the solid (force in solid per unit area of solid), and  $\mathbf{1}$  is the second-order identity tensor. We note that the intrinsic solid stress has the form

$$\boldsymbol{\sigma}_s = -p_s \mathbf{1} + \mathbf{s}_s, \quad (17)$$

where  $p_s$  is the intrinsic solid pressure and  $\mathbf{s}_s$  is the deviatoric component of  $\boldsymbol{\sigma}_s$ . However, it is also common knowledge that part of the total stress tensor  $\boldsymbol{\sigma}$  may be ascribed to an effective stress  $\boldsymbol{\sigma}'$  that depends on solely on the deformation of the solid frame. For linear elasticity, the relation takes the form

$$\boldsymbol{\sigma}' = \mathbb{C}^e : \boldsymbol{\epsilon}, \quad (18)$$

where  $\boldsymbol{\epsilon}$  is the small strain tensor describing the deformation of the solid frame, and  $\mathbb{C}^e$  is a rank-four tensor (with major and minor symmetries) characterizing the elastic isotropy or anisotropy of the porous material, see Sect. 4.

To determine the component of fluid pressure  $p$  that complements the effective stress  $\boldsymbol{\sigma}'$ , we make use of the principle of superposition shown in Fig. 1. In loading configuration (a) of this figure, the porous volume is subjected to a total stress of  $(\boldsymbol{\sigma} + p\mathbf{1})$  with no internal fluid pressure within the pores, thus resembling a dry condition. In this case, the load is borne completely by the solid frame. In loading configuration (b), on the other hand, a total stress of  $-p\mathbf{1}$  is applied to the same volume that generates an internal fluid pressure  $p$  within it. This second load is borne completely by the solid constituent. Superposition of these two loading configurations yields the original problem.

Since the internal fluid pressure is zero for loading configuration (a), the strain in the solid matrix can be calculated as

$$\boldsymbol{\epsilon}^{(a)} = (\mathbb{C}^e)^{-1} : (\boldsymbol{\sigma} + p\mathbf{1}), \quad (19)$$

where  $(\mathbb{C}^e)^{-1}$  is the elastic compliance tensor under dry (or drained) condition. For loading configuration (b), on the other hand, the solid matrix is subjected to isotropic deformation equal to the isotropic strain in the solid constituent, *i.e.*,

$$\boldsymbol{\epsilon}^{(b)} = -\frac{p}{3K_s} \mathbf{1}. \quad (20)$$

The sum of these two strains represents the total strain in the solid frame, *i.e.*,

$$\boldsymbol{\epsilon} = \boldsymbol{\epsilon}^{(a)} + \boldsymbol{\epsilon}^{(b)} = (\mathbb{C}^e)^{-1} : (\boldsymbol{\sigma} + p\mathbf{1}) - \frac{p}{3K_s} \mathbf{1}. \quad (21)$$

Pre-multiplying both sides by  $\mathbb{C}^e$  yields the effective Cauchy stress,

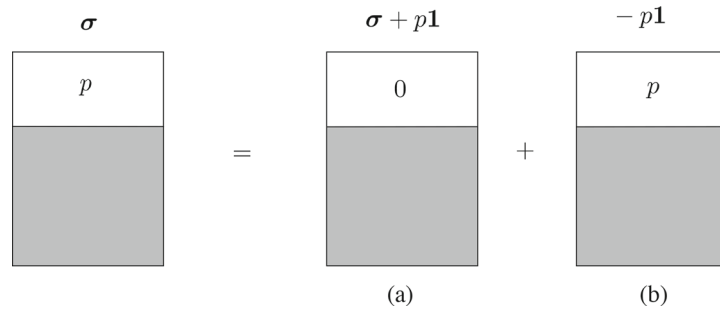


**Fig. 1** Superposition in poroelasticity: Phase diagram for a single-porosity volume with solid represented by the shaded area and pores represented by the white area. Volume is subjected to a tensorial stress indicated above each diagram; number inside the white area is the generated pore fluid pressure

$$\sigma' = \mathbb{C}^e : \epsilon = \sigma + p\mathbf{1} \quad \Rightarrow \quad \sigma = \sigma' - p\mathbf{1}, \quad (22)$$

where

$$\mathbf{b} = \mathbf{1} - \frac{\mathbb{C}^e : \mathbf{1}}{3K_s} \quad (23)$$

is the same Biot tensor derived by Zhao and Borja [58]. However, it must be noted that Zhao and Borja employed continuum thermodynamics to arrive at the above result, whereas the present formulation makes use of the superposition principle. That the same result is obtained via two different methods is noteworthy since one result verifies the other, see also the expression derived by Cheng [17]. We note that for isotropic elasticity the Biot tensor reduces to

$$\mathbf{b} = \left(1 - \frac{K}{K_s}\right)\mathbf{1} = \alpha\mathbf{1}, \quad (24)$$

where  $K$  is the elastic bulk modulus of the solid frame and  $\alpha = 1 - K/K_s$  is the familiar Biot coefficient, see Borja [10]. For rocks, typical values of  $\alpha$  range from 0.6 to 0.9 [39].

We next use the same superposition principle to evaluate the remaining dependent variable in the balance of mass for the solid phase, namely, either the mass density  $\rho_s$  in Eq. (7) or the pressure  $p_s$  in Eq. (10). Let us first define  $\theta_s$  as the intrinsic volumetric strain in the solid constituent, which can be decomposed into  $\theta_s^{(a)}$  and  $\theta_s^{(b)}$  following the superposition procedure. For loading configuration (a) shown in Fig. 1, the intrinsic Cauchy stress in the solid constituent is  $(\sigma + p\mathbf{1})/\phi^s$ , while the intrinsic mean normal stress is  $(\sigma + p)/\phi^s$ , where  $\sigma = \text{tr}(\boldsymbol{\sigma})/3$ . Thus, the intrinsic volumetric strain in the solid (assuming a constant  $K_s$ ) is

$$\theta_s^{(a)} = \frac{1}{K_s} \frac{\sigma + p}{\phi^s} = \frac{1}{K_s} \frac{-\phi^s p_s - \phi^f p + p}{\phi^s} = \frac{p - p_s}{K_s}. \quad (25)$$

For loading configuration (b), the solid constituent is subjected to the fluid pressure  $p$ , so

$$\theta_s^{(b)} = -\frac{p}{K_s}. \quad (26)$$

Adding the two and taking the material time derivative following the solid motion yields

$$\begin{aligned} \frac{d\theta_s}{dt} &= \frac{d\theta_s^{(a)}}{dt} + \frac{d\theta_s^{(b)}}{dt} \\ &= \frac{1}{\phi^s K_s} \left[ \frac{d\sigma}{dt} + \phi^f \frac{dp}{dt} - (p - p_s) \frac{d\phi^s}{dt} \right]. \end{aligned} \quad (27)$$

From solid mechanics, we know the intrinsic volumetric strain rate in solid  $d\theta_s/dt$  is related to the change in  $\rho_s$  through the following equation, assuming the solid mass is conserved

$$\frac{d\theta_s}{dt} = -\frac{1}{\rho_s} \frac{d\rho_s}{dt}. \quad (28)$$

After substituting Eqs. (27) and (28) into Eq. (7) and collecting terms, we obtain

$$\left(1 + \frac{p - p_s}{K_s}\right) \frac{d\phi^s}{dt} - \frac{1}{K_s} \left(\frac{d\sigma}{dt} + \phi^f \frac{dp}{dt}\right) + \phi^s \nabla \cdot \mathbf{v} = 0. \quad (29)$$

We note that

$$\frac{p - p_s}{K_s} = \theta_s^{(a)} \ll 1, \quad (30)$$

see [58]. Thus, the balance of mass for solid takes the simpler form

$$\frac{d\phi^s}{dt} - \frac{1}{K_s} \left(\frac{d\sigma}{dt} + \phi^f \frac{dp}{dt}\right) + \phi^s \nabla \cdot \mathbf{v} = 0. \quad (31)$$

The final step is to determine an expression for  $d\sigma/dt$ .

From the effective stress relation Eq. (22), we obtain

$$\frac{\mathbf{1} : \mathbb{C}^e : \epsilon}{3} = \sigma + \left(1 - \frac{\mathbf{1} : \mathbb{C}^e : \mathbf{1}}{9K_s}\right)p \quad (32)$$

by taking the trace of both sides. Next, by taking the

material time derivatives of both sides and solving, we obtain

$$\frac{d\sigma}{dt} = \frac{\mathbf{1} : \mathbb{C}^e}{3} : \frac{d\epsilon}{dt} - \left( 1 - \frac{\mathbf{1} : \mathbb{C}^e : \mathbf{1}}{9K_s} \right) \frac{dp}{dt}. \tag{33}$$

Substituting back into Eq. (31) and collecting terms yields

$$\frac{d\phi^s}{dt} + \frac{\beta}{K_s} \frac{dp}{dt} - \frac{\mathbf{1} : \mathbb{C}^e}{3K_s} : \frac{d\epsilon}{dt} + \phi^s \nabla \cdot \mathbf{v} = 0, \tag{34}$$

where

$$\beta = 1 - \phi^f - \frac{\mathbf{1} : \mathbb{C}^e : \mathbf{1}}{9K_s}. \tag{35}$$

For the fluid phase, we add Eqs. (14) and (34) to obtain

$$\mathbf{b} : \frac{d\epsilon}{dt} + \frac{1}{\mathcal{M}} \frac{dp}{dt} + \frac{1}{K_f} (\nabla p) \cdot \mathbf{q} + \nabla \cdot \mathbf{q} = 0, \tag{36}$$

where  $\mathcal{M}$  is the Biot modulus, defined as

$$\frac{1}{\mathcal{M}} = \frac{\beta}{K_s} + \frac{\phi^f}{K_f}. \tag{37}$$

Equation (36) can be used in combination with balance of linear momentum to solve coupled systems with the  $\mathbf{u}/p$  formulation [51, 58].

### 3 Double-porosity media

We denote by  $V$  a representative elementary volume (REV) consisting of a mixture of solid with double porosity. Let  $\phi^s$ ,  $\phi^m$ , and  $\phi^M$  represent the volume fractions of solid, nanopores, and micro-fractures, respectively, defined as

$$\phi^s = \frac{V_s}{V}, \quad \phi^m = \frac{V_m}{V}, \quad \phi^M = \frac{V_M}{V}, \tag{38}$$

where  $V_s$ ,  $V_m$ , and  $V_M$  are the volumes of solid, nanopores, and micro-fractures contained in  $V$ . The closure condition on the volume fractions is

$$\phi^s + \phi^m + \phi^M = 1. \tag{39}$$

The pore fractions represent the proportion of pore volume occupied by the nanopores and micro-fractures and are given by

$$\psi^m = \frac{\phi^m}{1 - \phi^s}, \quad \psi^M = \frac{\phi^M}{1 - \phi^s}. \tag{40}$$

The denominator in these two expressions,  $1 - \phi^s$ , is the porosity  $\phi$  of the mixture. The closure condition on the pore fractions is

$$\psi^m + \psi^M = 1. \tag{41}$$

In what follows, we assume that the nanopores and micro-

fractures are filled with the same type of fluid, which could be either liquid or gas. The partial mass densities of the solid, fluid in the nanopores, and fluid in the micro-fractures are given by

$$\rho^s = \phi^s \rho_s, \quad \rho^m = \phi^m \rho_m, \quad \rho^M = \phi^M \rho_M, \tag{42}$$

where  $\rho_s$ ,  $\rho_m$ , and  $\rho_M$  are the intrinsic mass densities of the solid, fluid in the nanopores, and fluid in the micro-fractures, respectively. The total mass density of the mixture is given by the sum

$$\rho = \rho^s + \rho^m + \rho^M. \tag{43}$$

Denoting the material time derivatives following the motions of solid and fluids by  $d(\cdot)/dt$ ,  $d^m(\cdot)/dt$ , and  $d^M(\cdot)/dt$ , the mass balance equations take the form

$$\frac{d\rho^s}{dt} + \rho^s \nabla \cdot \mathbf{v} = 0, \tag{44}$$

$$\frac{d^m \rho^m}{dt} + \rho^m \nabla \cdot \mathbf{v}_m = c^m, \tag{45}$$

$$\frac{d^M \rho^M}{dt} + \rho^M \nabla \cdot \mathbf{v}_M = c^M, \tag{46}$$

where  $\mathbf{v}$ ,  $\mathbf{v}_m$ , and  $\mathbf{v}_M$  are the velocities of solid, fluid in the nanopores, and fluid in the micro-fractures, respectively. We assume in the foregoing equations that the solid mass is conserved, and that the nanopores and micro-fractures exchange mass at the rates if  $c^m$  and  $c^M$  per unit total volume. For a closed system,

$$c^m + c^M = 0. \tag{47}$$

Assuming barotropic flow on the solid and fluids once again, we can write the solid mass balance equation in terms of  $\theta_s$  defined in Sect. 2 as

$$\frac{d\phi^s}{dt} - \phi^s \frac{d\theta_s}{dt} + \phi^s \nabla \cdot \mathbf{v} = 0, \tag{48}$$

and the fluid mass balance equations in terms of the intrinsic fluid pressures  $p_m$  and  $p_M$  as

$$\begin{aligned} \frac{d\phi^m}{dt} + \frac{\phi^m}{K_m} \frac{dp_m}{dt} + \frac{1}{K_m} (\nabla p_m) \cdot \mathbf{q}_m + \nabla \cdot \mathbf{q}_m \\ + \phi^m \nabla \cdot \mathbf{v} = \frac{c^m}{\rho_m}, \end{aligned} \tag{49}$$

$$\begin{aligned} \frac{d\phi^M}{dt} + \frac{\phi^M}{K_M} \frac{dp_M}{dt} + \frac{1}{K_M} (\nabla p_M) \cdot \mathbf{q}_M + \nabla \cdot \mathbf{q}_M \\ + \phi^M \nabla \cdot \mathbf{v} = \frac{c^M}{\rho_M}, \end{aligned} \tag{50}$$

where

$$\mathbf{q}_m = \phi^m (\mathbf{v}_m - \mathbf{v}), \quad \mathbf{q}_M = \phi^M (\mathbf{v}_M - \mathbf{v}) \tag{51}$$

are the superficial Darcy velocities; and  $K_m$  and  $K_M$  are the intrinsic fluid bulk moduli.

To derive the effective stress equation, a key aspect is to recognize the statistically distributed nature of the pores, which allows the double-porosity structure to be represented by a single-porosity structure with a weighted pore fluid pressure. Consider, for example, the superposition shown in Fig. 2. Here, the double-porosity structure is replaced with a statistically equivalent single-porosity structure with a weighted pore fluid pressure of  $\bar{p}$  given by [11]

$$\bar{p} = \psi^M p_M + \psi^m p_m. \tag{52}$$

Thus, we can use the results from Sect. 2 directly by replacing  $p$  with  $\bar{p}$  rather than repeating the whole process of Sect. 2. Specifically, from Eq. (22), we have

$$\boldsymbol{\sigma} = \boldsymbol{\sigma}' - \bar{p}\mathbf{b} = \boldsymbol{\sigma}' - \psi^M p_M \mathbf{b} - \psi^m p_m \mathbf{b}, \tag{53}$$

where  $\mathbf{b}$  is the same Biot tensor given in Eq. (23). From Eq. (34), we have

$$\frac{d\phi^s}{dt} + \frac{\beta}{K_s} \frac{d\bar{p}}{dt} - \frac{\mathbf{1} : \mathbb{C}^e}{3K_s} : \frac{d\boldsymbol{\epsilon}}{dt} + \phi^s \nabla \cdot \mathbf{v} = 0, \tag{54}$$

where  $\beta$  is already defined in Eq. (35) with  $\phi^f$  replaced by total porosity  $\phi = \phi^M + \phi^m$ . Note here the time derivative of  $\bar{p}$  generates an additional term which is the time derivative of pore fraction  $d\psi^M/dt$ , and this term is unique to double-porosity formulation.

**Remark** An alternative approach that does not explicitly employ volume averaging of the pore pressures, such as that shown in Eq. (52), is presented in “Appendix”. This latter formulation reinforces the understanding that the principle of superposition does not depend on the sequence of loading, and that there is more than one way by which one can get to the same result.

In order to evaluate  $d\phi^m/dt$  and  $d\phi^M/dt$  of Eqs. (49) and (50), we must develop a constitutive law for  $d\psi^M/dt$ . We refer to the phase diagram shown in Fig. 3, where the

REV is partitioned into two superimposed regions representing the nanopore and micro-fracture skeletons. These two regions must be distinguished from the nanopore and micro-fracture volumes, which are mainly pore spaces occupied by fluids. The nanopore and micro-fracture skeletons are themselves superimposed solids and pore spaces. Let  $V_{np}$  and  $V_{mf}$  represent respective portions of the total volume  $V$  occupied by the nanopore and micro-fracture skeletons. The corresponding volume fractions are

$$\phi^m = \frac{V_{np}}{V}, \quad \phi^M = \frac{V_{mf}}{V}, \quad \phi^m + \phi^M = 1. \tag{55}$$

Since both volume fractions are statistically distributed throughout the entire volume, we would require the porosities are the same for the nanopore and micro-fracture skeletons, *i.e.*,

$$\frac{\phi^m}{\phi^m} = \frac{\phi^M}{\phi^M}, \tag{56}$$

which implies that  $\phi^m \equiv \psi^m$  and  $\phi^M \equiv \psi^M$ .

We next consider following trivial decomposition

$$\boldsymbol{\sigma} = \psi^m \boldsymbol{\sigma}' + \psi^M \boldsymbol{\sigma}', \tag{57}$$

and assume the following decomposition for  $\boldsymbol{\sigma}'$

$$\boldsymbol{\sigma}' = \psi^m \boldsymbol{\sigma}'_m + \psi^M \boldsymbol{\sigma}'_M, \tag{58}$$

where  $\boldsymbol{\sigma}'_m$  and  $\boldsymbol{\sigma}'_M$  are effective stresses in the nanopore and micro-fracture skeletons of Fig. 3. Rewriting the effective stress relation Eq. (53) in the expanded form using above two equations gives

$$\psi^m (\boldsymbol{\sigma} + p_m \mathbf{b}) + \psi^M (\boldsymbol{\sigma} + p_M \mathbf{b}) = \psi^m \boldsymbol{\sigma}'_m + \psi^M \boldsymbol{\sigma}'_M. \tag{59}$$

This equation holds for any  $\psi^M$  (and  $\psi^m$ ), so we must have

$$\boldsymbol{\sigma} + p_m \mathbf{b} = \boldsymbol{\sigma}'_m, \quad \boldsymbol{\sigma} + p_M \mathbf{b} = \boldsymbol{\sigma}'_M, \tag{60}$$

which means that

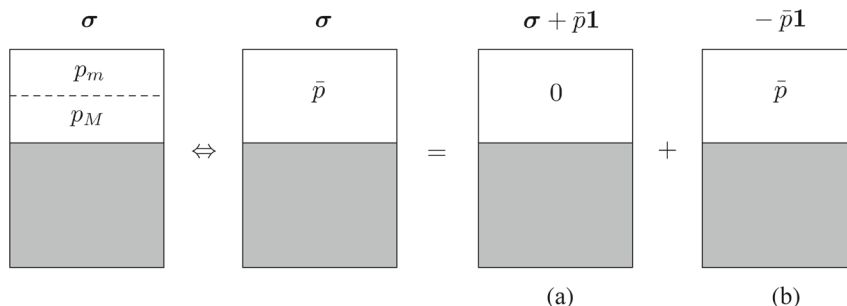


**Fig. 2** Statistically distributed pores allow a double-porosity structure to be replaced with a single-porosity structure with mean pore fluid pressure  $\bar{p}$

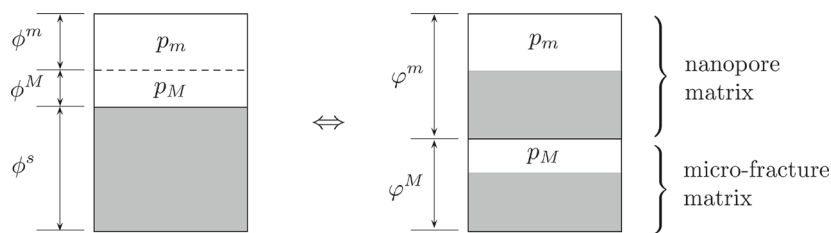


**Fig. 3** Representation of double-porosity structure in terms of superimposed nanopore and micro-fracture skeletons or matrices

$$\sigma'_m - p_m \mathbf{b} = \sigma'_M - p_M \mathbf{b}. \tag{61}$$

Taking the trace and applying the material time derivative with respect to solid motion gives

$$\frac{d\sigma'_m}{dt} - \frac{d\sigma'_M}{dt} = \left( \frac{dp_m}{dt} - \frac{dp_M}{dt} \right) b, \tag{62}$$

where  $\sigma'_m = \text{tr}(\sigma'_m)/3$ ,  $\sigma'_M = \text{tr}(\sigma'_M)/3$ , and  $b = \text{tr}(\mathbf{b})/3$ .

In terms of the volumetric strain in the nanopore and micro-fracture skeletons,  $\theta_m$  and  $\theta_M$ , respectively, we assume linear elasticity and rewrite the foregoing equations as

$$K_m^e \frac{d\theta_m}{dt} - K_M^e \frac{d\theta_M}{dt} = \left( \frac{dp_m}{dt} - \frac{dp_M}{dt} \right) b, \tag{63}$$

where  $K_m^e$  and  $K_M^e$  are the elastic bulk moduli of the nanopore and micro-fracture skeletons, respectively (not to be confused with the fluid bulk moduli  $K_m$  and  $K_M$ ). Finally, from Fig. 3, we recognize that if the height of the REV remains unchanged, we can represent  $d\theta_m/dt$  and  $d\theta_M/dt$  as

$$\frac{d\theta_m}{dt} = -\frac{1}{1 - \psi^M} \frac{d\psi^M}{dt}, \quad \frac{d\theta_M}{dt} = \frac{1}{\psi^M} \frac{d\psi^M}{dt}. \tag{64}$$

Substituting Eqs. (64) into (63) yields the poroelastic equation

$$\frac{d\psi^M}{dt} = \frac{1}{C} \left( \frac{dp_M}{dt} - \frac{dp_m}{dt} \right), \tag{65}$$

where

$$C = \frac{1}{b} \left( \frac{K_m^e}{1 - \psi^M} + \frac{K_M^e}{\psi^M} \right) \tag{66}$$

is a modulus describing the change in internal structure of the material. We remark that a constitutive law relating the variation of pore fraction  $\psi^M$  with pore pressure difference  $p_M - p_m$  is consistent with the internal energy equation for double-porosity media developed by Borja and Choo [13]. We also note that only one combined coefficient  $C$  is needed to describe the material response, although its physical meaning is based on the two elasticity constants  $K_m^e$  and  $K_M^e$ .

Now, we can rewrite Eqs. (49) and (50) in terms of the primary unknown variables  $p_m$ ,  $p_M$ , and  $\epsilon$ . Recall that

$$\frac{d\phi^m}{dt} = -\psi^m \frac{d\phi^s}{dt} - \phi \frac{d\psi^M}{dt} \tag{67}$$

and

$$\frac{d\phi^M}{dt} = -\psi^M \frac{d\phi^s}{dt} + \phi \frac{d\psi^M}{dt}. \tag{68}$$

Thus, we can combine Eqs. (54) and (65) to obtain equivalent forms of Eqs. (49) and (50) as

$$\begin{aligned} \psi^m \mathbf{b} : \frac{d\epsilon}{dt} + \frac{1}{K_m} (\nabla p_m) \cdot \mathbf{q}_m + \nabla \cdot \mathbf{q}_m \\ + S_{mM} \frac{dp_M}{dt} + S_{mm} \frac{dp_m}{dt} = \frac{c^m}{\rho_m} \end{aligned} \tag{69}$$

and

$$\begin{aligned} \psi^M \mathbf{b} : \frac{d\epsilon}{dt} + \frac{1}{K_M} (\nabla p_M) \cdot \mathbf{q}_M + \nabla \cdot \mathbf{q}_M \\ + S_{MM} \frac{dp_M}{dt} + S_{Mm} \frac{dp_m}{dt} = \frac{c^M}{\rho_M}. \end{aligned} \tag{70}$$

where

$$\left. \begin{aligned} S_{mm} &= \frac{\beta \psi^m \psi^m}{K_s} + \frac{\phi^m}{K_m} - \frac{\omega^m - \phi}{C} \\ S_{MM} &= \frac{\beta \psi^M \psi^M}{K_s} + \frac{\phi^M}{K_M} + \frac{\omega^M + \phi}{C} \\ S_{mM} &= \frac{\beta \psi^m \psi^M}{K_s} + \frac{\omega^m - \phi}{C} \\ S_{Mm} &= \frac{\beta \psi^M \psi^M}{K_s} - \frac{\omega^M + \phi}{C} \end{aligned} \right\} \tag{71}$$

are storage coefficients. Equations (69) and (70) can then be used in combination with balance of linear momentum to solve coupled systems based on a  $\mathbf{u}/p_M/p_m$  formulation [18, 19, 56].

In calculating the coefficients of Eqs. (69) and (70), we can further assume that

$$\begin{aligned} \omega^m &= \frac{\beta(p_M - p_m)\psi^m}{K_s} \ll 1, \\ \omega^M &= \frac{\beta(p_M - p_m)\psi^M}{K_s} \ll 1, \end{aligned} \tag{72}$$

since  $|p_M - p_m|/K_s$  is on the order of intrinsic strain [9]. In this case, the storage coefficients reduce to the forms

$$\left. \begin{aligned} S_{mm} &= \frac{\beta\psi^m\psi^m}{K_s} + \frac{\phi^m}{K_m} + \frac{\phi}{C} \\ S_{MM} &= \frac{\beta\psi^M\psi^M}{K_s} + \frac{\phi^M}{K_M} + \frac{\phi}{C} \\ S_{mM} &= S_{Mm} = \frac{\beta\psi^m\psi^M}{K_s} - \frac{\phi}{C} \end{aligned} \right\}, \tag{73}$$

i.e., the matrix of storage coefficients becomes symmetric. Thus, all the coefficients of  $d\epsilon/dt$ ,  $dp_M/dt$ , and  $dp_m/dt$  are “constants” in the sense that they do not depend on the primary unknown variables. Furthermore, it is also reasonable to assume that the pressures  $p_M$  and  $p_m$  do not affect the density terms in  $\mathbf{q}_M$  and  $\mathbf{q}_m$ , i.e.,  $\mathbf{q}_M = \mathbf{q}_M(\nabla p_M, \rho_{\text{ref}}\mathbf{g})$  and  $\mathbf{q}_m = \mathbf{q}_m(\nabla p_m, \rho_{\text{ref}}\mathbf{g})$ , where  $\rho_{\text{ref}}$  is the reference (constant) fluid density and  $\mathbf{g}$  is the gravity acceleration vector.

Finally, we can combine Eqs. (69) and (70) to obtain the total flow equation. The result reads

$$\begin{aligned} \mathbf{b} : \frac{d\epsilon}{dt} + \frac{1}{\mathcal{M}_m} \frac{dp_m}{dt} + \frac{1}{\mathcal{M}_M} \frac{dp_M}{dt} + \frac{1}{K_m} (\nabla p_m) \cdot \mathbf{q}_m \\ + \frac{1}{K_M} (\nabla p_M) \cdot \mathbf{q}_M + \nabla \cdot \mathbf{q}_t = \frac{c^m}{\rho_m} + \frac{c^M}{\rho_M}, \end{aligned} \tag{74}$$

where  $\mathcal{M}_m$  and  $\mathcal{M}_M$  are the Biot moduli defined as

$$\begin{aligned} \frac{1}{\mathcal{M}_m} &= \left( \frac{\beta}{K_s} + \frac{\phi}{K_m} \right) \psi^m - \frac{\beta(p_M - p_m)}{K_s C}, \\ \frac{1}{\mathcal{M}_M} &= \left( \frac{\beta}{K_s} + \frac{\phi}{K_M} \right) \psi^M + \frac{\beta(p_M - p_m)}{K_s C}, \end{aligned} \tag{75}$$

$\phi$  is the porosity, and  $\mathbf{q}_t = \mathbf{q}_m + \mathbf{q}_M$  is the resultant total flux vector. Eq. (74) is analogous to the pressure equation of multiphase flow through porous media [48].

## 4 Poroelastic coefficients

### 4.1 Elastic coefficients

Before illustrating how Eqs. (69) and (70) may be used, we first consider a transversely isotropic elastic solid characterized by an elastic moduli tensor  $\mathbb{C}^e$  of the form

$$\begin{aligned} \mathbb{C}^e &= \lambda^e \mathbf{1} \otimes \mathbf{1} + 2\mu_T \mathbb{I} + a^e (\mathbf{1} \otimes \mathbf{M} + \mathbf{M} \otimes \mathbf{1}) \\ &+ b^e \mathbf{M} \otimes \mathbf{M} + 2(\mu_L - \mu_T) (\mathbf{M} \odot \mathbf{1} + \mathbf{1} \odot \mathbf{M}), \end{aligned} \tag{76}$$

where  $(\mathbf{A} \odot \mathbf{B})_{ijkl} = (A_{ik}B_{jl} + A_{il}B_{jk})/2$ ,  $\mathbb{I}$  is the symmetric fourth-order identity tensor,  $\mathbf{M} = \mathbf{n} \otimes \mathbf{n}$  is the microstructure tensor,  $\mathbf{n}$  is the unit normal vector to the bedding plane, and  $\lambda^e$ ,  $\mu_L$ ,  $\mu_T$ ,  $a^e$ , and  $b^e$  are the five material elastic constants. The subscript  $(\cdot)_T$  (bed-parallel BP) pertains to the plane of isotropy, and subscript  $(\cdot)_L$  (bed-normal BN) pertains to the direction perpendicular to the plane of isotropy.

In practice, we do not determine  $\lambda^e$ ,  $\mu_L$ ,  $\mu_T$ ,  $a^e$ , and  $b^e$  directly from laboratory experiments. Instead, we obtain these constants indirectly from the following procedure. First, we perform the following matrix inversion

$$\begin{bmatrix} \mathbb{C}_{11}^e & \mathbf{0} \\ \mathbf{0} & \mathbb{C}_{22}^e \end{bmatrix} = \begin{bmatrix} \mathbb{S}_{11}^e & \mathbf{0} \\ \mathbf{0} & \mathbb{S}_{22}^e \end{bmatrix}^{-1}, \tag{77}$$

where  $\mathbf{0}$  represents a  $3 \times 3$  null matrix. The remaining submatrices are

$$\mathbb{C}_{11}^e = \begin{bmatrix} \lambda^e + 2\mu_T & \lambda^e & \lambda^e + a^e \\ \lambda^e & \lambda^e + 2\mu_T & \lambda^e + a^e \\ \lambda^e + a^e & \lambda^e + a^e & \lambda^e + 2\tilde{\mu} \end{bmatrix}, \tag{78}$$

where  $\tilde{\mu} = 2\mu_L - \mu_T + a^e + b^e/2$ , and

$$\mathbb{C}_{22}^e = \begin{bmatrix} \mu_T & 0 & 0 \\ 0 & \mu_L & 0 \\ 0 & 0 & \mu_L \end{bmatrix}. \tag{79}$$

The compliance submatrices are

$$\mathbb{S}_{11}^e = \begin{bmatrix} 1/E_h & -v_{hh}/E_h & -v_{vh}/E_v \\ -v_{hh}/E_h & 1/E_h & -v_{vh}/E_v \\ -v_{hv}/E_h & -v_{hv}/E_h & 1/E_v \end{bmatrix} \tag{80}$$

and

$$\mathbb{S}_{22}^e = \begin{bmatrix} 2(1 + v_{hh})/E_h & 0 & 0 \\ 0 & 1/G_{vh} & 0 \\ 0 & 0 & 1/G_{vh} \end{bmatrix}. \tag{81}$$

In the above four submatrices,  $E_v$  and  $E_h$  are Young’s moduli in  $v$  and  $h$  directions,  $v_{hh}$ ,  $v_{vh}$ , and  $v_{hv}$  are Poisson’s ratios, and  $G_{vh}$  is the shear modulus. These constants are directly measurable in laboratory experiments [38]. Poisson’s ratios  $v_{hv}$  and  $v_{vh}$  are not independent because we have

$$\frac{v_{vh}}{E_v} = \frac{v_{hv}}{E_h}, \tag{82}$$

which guarantees symmetry of the compliance matrix. Note the matrix on the LHS of Eq. (77) is exactly the Voigt form of  $\mathbb{C}^e$  in Eq. (76) when  $\mathbf{n} = \mathbf{e}_z = [0, 0, 1]^T$ .



### 4.2 Comparison of poroelastic coefficients

To further illustrate the use of formulas (69) and (70), we compare the calculated values of the poroelastic coefficients with those obtained by Berryman and Pride [8] and Khalili and Selvadurai [29]. To this end, we elucidate the differences in the mathematical formulations adopted in their models. Berryman and Pride considered an isotropic double-porosity material with six basic variables, namely, the mean total stress  $\sigma$ , volumetric strain  $\epsilon$ , fluid pressures  $p_M$  and  $p_m$ , and fluid content variations  $\zeta_M$  and  $\zeta_m$ . In terms of these variables, they formulated a set of linear constitutive equations of the form

$$\begin{pmatrix} \epsilon \\ -\zeta_m \\ -\zeta_M \end{pmatrix} = \begin{bmatrix} a_{11} & a_{12} & a_{13} \\ a_{12} & a_{22} & a_{23} \\ a_{13} & a_{23} & a_{33} \end{bmatrix} \begin{pmatrix} \sigma \\ -p_m \\ -p_M \end{pmatrix}, \tag{83}$$

where  $a_{11}$  through  $a_{33}$  are all constant coefficients. The flow continuity equations are given as [37]

$$\frac{\partial \zeta_m}{\partial t} + \nabla \cdot \mathbf{q}_m = \gamma(p_M - p_m), \tag{84}$$

$$\frac{\partial \zeta_M}{\partial t} + \nabla \cdot \mathbf{q}_M = \gamma(p_m - p_M), \tag{85}$$

where  $\gamma$  is the leakage parameter. This approach is a phenomenological or micromechanical approach for obtaining the poroelastic coefficients, which is different from what we have presented in Sect. 3.

In order to rewrite Eqs. (84) and (85) in terms of the primary unknown variables adopted in our formulation, we need to move the term  $\sigma$  in Eq. (83) to the LHS and the term  $\epsilon$  to the RHS. The result reads

$$\sigma = \frac{\epsilon}{a_{11}} + \frac{a_{12}}{a_{11}}p_m + \frac{a_{13}}{a_{11}}p_M, \tag{86}$$

$$\zeta_m = -\frac{a_{12}}{a_{11}}\epsilon + s_{mm}p_m + s_{mM}p_M, \tag{87}$$

and

$$\zeta_M = -\frac{a_{13}}{a_{11}}\epsilon + s_{Mm}p_m + s_{MM}p_M. \tag{88}$$

where the storage coefficients are given by

$$\left. \begin{aligned} s_{mm} &= a_{22} - \frac{a_{12}^2}{a_{11}} \\ s_{MM} &= a_{33} - \frac{a_{13}^2}{a_{11}} \\ s_{mM} &= s_{Mm} = a_{23} - \frac{a_{12}a_{13}}{a_{11}} \end{aligned} \right\}. \tag{89}$$

From the above three equations, we identify the scalar Biot coefficients of the Berryman–Pride isotropic double-porosity model as  $-a_{12}/a_{11}$  (for nanopores or matrix) and

$-a_{13}/a_{11}$  (for micro-fractures). As for the formulation proposed by Khalili and Selvadurai [29], we tune the values of  $K_p$  (bulk modulus of the porous blocks),  $K_b$ , and  $K_s$  in their formulation so as to obtain the same Biot coefficients  $-a_{12}/a_{11}$  and  $-a_{13}/a_{11}$  of the Berryman–Pride model. The result reads

$$K_b = \frac{1}{a_{11}}, \quad K_p = \frac{K_b}{1 + (a_{13}/a_{11})}, \quad K_s = \frac{1}{a_{11} + a_{12} + a_{13}}. \tag{90}$$

while the fluid content variations are given by

$$\zeta_m = \alpha_1\epsilon + \mathring{s}_{mM}p_M + \mathring{s}_{mm}p_m \tag{91}$$

and

$$\zeta_M = \alpha_2\epsilon + \mathring{s}_{Mm}p_m + \mathring{s}_{MM}p_M, \tag{92}$$

where the storage coefficients are

$$\left. \begin{aligned} \mathring{s}_{mm} &= \frac{\alpha_2 - \phi^M}{K_p} + \frac{\alpha_1 - \phi^m - \alpha_2 + \phi^M}{K_s} + \frac{\phi^m}{K_m} \\ \mathring{s}_{MM} &= \frac{\alpha_2 - \phi^M}{K_p} + \frac{\phi^M}{K_M} \\ \mathring{s}_{mM} &= \mathring{s}_{Mm} = \frac{\alpha_2 - \phi^M}{K_s} - \frac{\alpha_2 - \phi^M}{K_p} \end{aligned} \right\}, \tag{93}$$

and where  $\alpha_1 = K_b/K_p - K_b/K_s = -a_{12}/a_{11}$  and  $\alpha_2 = 1 - K_b/K_p = -a_{13}/a_{11}$ . Note that we have modified the notation for  $\zeta_m$  and  $\zeta_M$  to indicate that the Khalili–Selvadurai constitutive formulation is not the same as the Berryman–Pride formulation. By substituting these constitutive laws into Eqs. (84) and (85), it is now possible to compare the poroelastic coefficients with those used in Eqs. (69) and (70).

Table 1 presents a set of input parameters used in these constitutive relations. We consider two types of material, Chelmsford granite and Weber sandstone, since they are well-characterized by laboratory data. Tables 2, 3 and 4 display the results of calculations using the above three double-porosity frameworks. By comparing these three frameworks, we find that the Biot coefficients of our method are quite different from the other two methods, which is because we use pore fractions ( $\psi^M$  and  $\psi^m$ ) as weights to obtain  $\bar{p}$  in Fig. 2, while different weighting schemes were adopted in [8, 29]. Nevertheless, the total Biot coefficient matches well among the three methods. The main dependence on the last three rows of Table 2 (i.e., the storage coefficients, ignoring the  $\phi^m$  and  $\phi^M$  terms) is in the value of  $\mathcal{C}$ , and by tuning the value of  $\mathcal{C}$ , we find that the agreement of the storage coefficients with those of the other two methods is quite good for both the granite and sandstone examples. In particular, we find the off-diagonal storage coefficients  $S_{Mm}$ ,  $s_{Mm}$ , and  $\mathring{s}_{Mm}$  have a

negative value for both rocks, which might also be true for other parameter settings. Furthermore, it must be emphasized that our approach is the only one that can handle an anisotropic macroscopic system. In terms of the time derivative, our approach adopts the material time derivative for solid and fluid, while the other two approaches simply use partial time derivative as an approximation, compare Eqs. (69) and (70) with Eqs. (84) and (85), for example. This facilitates an easier extension of our theory to the finite deformation regime since the material time derivative already carries the convected term.

### 5 Closure

We have utilized the principle of superposition to derive proelastic coefficients for single- and double-porosity media. The resulting conservation laws are exact for single-porosity media and are consistent with those derived in [17, 58]. For double-porosity media, we derived an evolution law for total porosity  $\phi$  by introducing the weighted pore fluid pressure  $\bar{p} = \psi^M p_M + \psi^m p_m$  in the equivalent single-porosity structure, which is consistent with the results of Borja and Koliji [11]. We then adopted the effective stress partition concept to derive an evolution law for the pore fraction  $\psi^M$  or  $\psi^m$ . Identical results were obtained by using different loading paths, thus affirming

**Table 2** Double-porosity and state variables for the proposed formulation

Variable/coefficient	Granite	Sandstone
$\text{tr}(\psi^m \mathbf{b})/3$ for nanopores	0.077	0.812
$\text{tr}(\psi^M \mathbf{b})/3$ for micro-fractures	0.773	0.081
Intermediate variable $\beta$	0.838	0.788
Storage coefficient $S_{mm}$ (GPa <sup>-1</sup> )	0.025	0.079
Storage coefficient $S_{MM}$ (GPa <sup>-1</sup> )	0.040	0.036
Storage coefficient $S_{Mm}$ (GPa <sup>-1</sup> )	-0.023	-0.031

Note that the storage coefficients are multipliers of material time derivatives. Furthermore, the results in this table are invariant with respect to the vector  $\mathbf{n}$  given in Table 1

**Table 3** Berryman and Pride [8] double-porosity coefficients

Coefficient	Granite	Sandstone
$\alpha_1$ for nanopores	0.318	0.292
$\alpha_2$ for micro-fractures	0.533	0.600
Storage coefficient $s_{mm}$ (GPa <sup>-1</sup> )	0.028	0.078
Storage coefficient $s_{MM}$ (GPa <sup>-1</sup> )	0.034	0.062
Storage coefficient $s_{Mm}$ (GPa <sup>-1</sup> )	-0.022	-0.044

**Table 1** Material parameters

Parameter	Chelmsford granite	Weber sandstone
$a_{11}$ (GPa <sup>-1</sup> )	0.125	0.250
$a_{12}$ (GPa <sup>-1</sup> )	-0.040	-0.073
$a_{13}$ (GPa <sup>-1</sup> )	-0.067	-0.150
$a_{22}$ (GPa <sup>-1</sup> )	0.041	0.100
$a_{23}$ (GPa <sup>-1</sup> )	-0.0010	-0.0003
$a_{33}$ (GPa <sup>-1</sup> )	0.070	0.152
$K_s$ (GPa)	53.6	37.3
$K_m = K_M = K_f$ (GPa)	3.3	3.3
Porosity $\phi^m$	0.001	0.095
Porosity $\phi^M$	0.011	0.010
Young's modulus $E_h$ (GPa)	13.0	7.8
Young's modulus $E_v$ (GPa)	8.5	5.0
Shear modulus $G_{vh}$ (GPa)	4.0	3.0
Poisson's ratio $\nu_{hh}$	0.18	0.15
Poisson's ratio $\nu_{vh}$	0.25	0.20
Vector $\mathbf{n}$	$\mathbf{e}_z = [0, 0, 1]^T$	$\mathbf{e}_z = [0, 0, 1]^T$
Intermediate modulus $\mathcal{C}$ (GPa)	0.5	3.2

Note that Berryman and Pride [8] did not provide the values of  $E_h, E_v, G_{vh}, \nu_{hh}$ , and  $\nu_{vh}$ , so they were deduced by setting  $\mathbf{1} : \mathbb{C}^c : \mathbf{1}/9 \approx 1/a_{11}$ . In addition, they determined the values of  $a_{11}$  through  $a_{33}$  from a large number of other material parameters, see their Table 1 and Table B1

**Table 4** Khalili and Selvadurai [29] double-porosity coefficients

Coefficient	Granite	Sandstone
$\alpha_1$ for nanopores	0.318	0.292
$\alpha_2$ for micro-fractures	0.533	0.600
Storage coefficient $\hat{s}_{mm}$ (GPa <sup>-1</sup> )	0.027	0.077
Storage coefficient $\hat{s}_{MM}$ (GPa <sup>-1</sup> )	0.034	0.062
Storage coefficient $\hat{s}_{Mm}$ (GPa <sup>-1</sup> )	-0.021	-0.043

the invariance of the principle of superposition with respect to sequence of loading.

The resulting formulas for double-porosity media require fewer material parameters than those proposed by other authors while delivering a comparable performance. Thus, the proposed approach is useful whenever the unknown parameters cannot be readily determined in the laboratory. Provided that the processes involved are reversible, extension of this work to multi-field coupling, such as thermo-hydro-chemo-mechanical (THCM) coupling, is possible. However, the principle of superposition cannot be applied to irreversible or path-dependent processes, such as processes involving elastoplastic deformations. In this case, the formulation must be complemented by thermodynamical principles to accommodate the effect of plastic dissipation [12]. Nevertheless, the theory presented in this paper is still very useful for a wide variety of applications given the prominent role of poroelasticity in the scientific literature.

### Appendix: An alternative superposition

In this Appendix, we derive the effective stress equation using the principle of superposition but with an alternative sequence of loading on an elementary volume shown in Fig. 4. As noted earlier, the result should not depend on the sequence of loading, and here we illustrate a more

elaborate loading scenario than the one presented earlier. In loading configuration (a) of Fig. 4, the volume is subjected to a total stress of  $(\sigma + p_M \mathbf{1})$  with no internal fluid pressure in either the nanopores or the micro-fractures. The associated strain in the solid matrix is then calculated as

$$\epsilon^{(a)} = (\mathbb{C}^e)^{-1} : (\sigma + p_M \mathbf{1}), \tag{94}$$

where  $\mathbb{C}^e$  is the previously defined drained elasticity tensor for the double-porosity medium. For loading configuration (b), the solid matrix is subjected to isotropic deformation equal to the isotropic strain in the solid constituent, and so we write

$$\epsilon^{(b)} = -\frac{p_m}{3K_s} \mathbf{1}. \tag{95}$$

Loading configuration (c) shows the volume under an isotropic stress of  $-(p_M - p_m) \mathbf{1}$  with a pore fluid pressure of  $(p_M - p_m)$  acting in the micro-fractures and zero in the nanopores. Because both pore scales are statistically distributed throughout the entire volume, the loading is equivalent to having all of the pore spaces subjected to a uniform pressure of  $\psi^M(p_M - p_m)$ , which we further analyze in Fig. 5.

In Fig. 5, loading configuration (c) is replaced with loading configuration (d), which in turn is represented as the superposition of loading configurations (e) and (f). In loading configuration (e), the volume is subjected to a total load of  $-(1 - \psi^M)(p_M - p_m) \mathbf{1}$  with no pressure within the pores. This results in a drained isotropic deformation of the solid skeleton equal to

$$\epsilon^{(e)} = -(\mathbb{C}^e)^{-1} : (1 - \psi^M)(p_M - p_m) \mathbf{1}. \tag{96}$$

In loading configuration (f), the solid constituent is subjected to an isotropic deformation equal to the isotropic strain in the solid constituent, which is given by

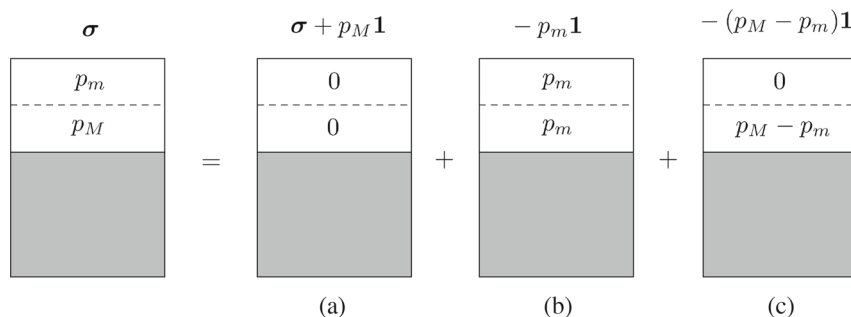


**Fig. 4** Superposition in poroelasticity: Phase diagram for a double-porosity volume with solid represented by the shaded area and pores represented by the white area. Volume is subjected to a tensorial stress indicated above each diagram; numbers inside the white area are the generated pore fluid pressures in the nanopores ( $p_m$ ) and micro-fractures ( $p_M$ )

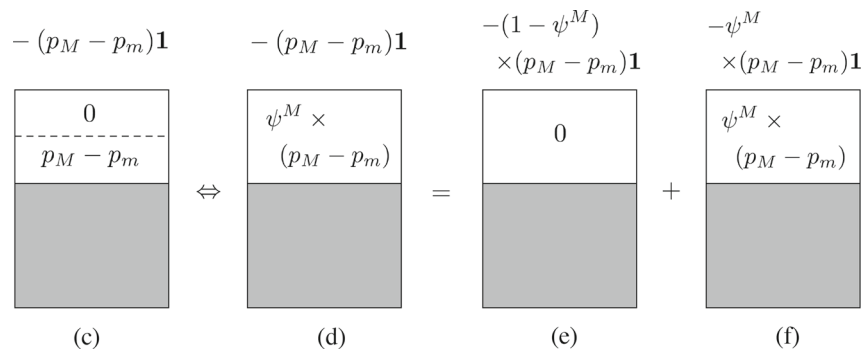


**Fig. 5** Superposition in poroelasticity: Phase diagram for a double-porosity volume with solid represented by the shaded area and pores represented by the white area. Loading configuration (c) is equivalent to loading configuration (d), which is represented as the superposition of loading configurations (e) and (f)

$$\epsilon^{(f)} = -\frac{\psi^M (p_M - p_m)}{3K_s} \mathbf{1}. \quad (97)$$

Adding all four components of strain yields the total strain in the solid frame, equal to

$$\begin{aligned} \epsilon &= \epsilon^{(a)} + \epsilon^{(b)} + \epsilon^{(e)} + \epsilon^{(f)} \\ &= (\mathbb{C}^e)^{-1} : (\boldsymbol{\sigma} + \bar{p} \mathbf{1}) - \frac{\bar{p}}{3K_s} \mathbf{1}, \end{aligned} \quad (98)$$

where  $\bar{p}$  is the same mean pore fluid pressure defined in Eq. (52). Premultiplying both sides by  $\mathbb{C}^e$  and noting once again that  $\mathbb{C}^e : \epsilon$  is the effective Cauchy stress  $\boldsymbol{\sigma}'$  yields Eq. (53).

**Acknowledgements** This material is based upon work supported by the U.S. Department of Energy, Office of Science, Office of Basic Energy Sciences, Geosciences Research Program, under Award Number DE-FG02-03ER15454. Support for materials and additional student hours were provided by the National Science Foundation under Award Number CMMI-1914780.

## References

- Ashworth M, Doster F (2019) Foundations and their practical implications for the constitutive coefficients of poromechanical dual-continuum models. *Transp Porous Media* 130:699–730
- Ashworth M, Doster F (2020) Anisotropic dual-continuum representations for multiscale poroelastic materials: development and numerical modeling. *Int J Numer Anal Methods Geomech* 44:2304–2328
- Bai M, Elsworth D (2000) Coupled processes in subsurface deformation, flow, and transport. ASCE Press, ASCE Book Series, Virginia
- Barenblatt GI, Zheltov IuP, Kochina IN (1960) Basic concepts in the theory of seepage of homogeneous liquids in fissured rocks [strata]. *J Appl Math Mech* 24:1286–1303
- Bennett KC, Berla LA, Nix WD, Borja RI (2015) Instrumented nanoindentation and 3D mechanistic modeling of a shale at multiple scales. *Acta Geotech* 10:1–14
- Berre I, Doster F, Keilegavlen E (2019) Flow in fractured porous media: a review of conceptual models and discretization approaches. *Transp Porous Media* 130:215–236
- Berryman JG (2002) Extension of poroelastic analysis to double-porosity materials: new technique in microgeomechanics. *J Eng Mech* 128:840–847
- Berryman JG, Pride SR (2002) Models for computing geomechanical constants of double-porosity materials from the constituents' properties. *J Geophys Res* 107:1–15
- Bonazzi A, Jha B, de Barros FJP (2021) Transport analysis in deformable porous media through integral transforms. *Int J Numer Anal Methods Geomech* 45:307–324
- Borja RI (2006) On the mechanical energy and effective stress in saturated and unsaturated porous continua. *Int J Solids Struct* 43:1764–1786
- Borja RI, Koliji A (2009) On the effective stress in unsaturated porous continua with double porosity. *J Mech Phys Solids* 57:1182–1193
- Borja RI (2013) *Plasticity Modeling & Computation*. Springer-Verlag, Berlin-Heidelberg
- Borja RI, Choo J (2016) Cam-Clay plasticity, Part VIII: A constitutive framework for porous materials with evolving internal structure. *Comput Methods Appl Mech Eng* 309:653–679
- Borja RI, Yin Q, Zhao Y (2020) Cam-Clay plasticity. Part IX: On the anisotropy, heterogeneity, and viscoplasticity of shale. *Comput Methods Appl Mech Eng* 360:112695
- Camargo JT, White JA, Borja RI (2021) A macroelement stabilization for mixed finite element/finite volume discretizations of multiphase poromechanics. *Comput Geosci* 25:775–792
- Chen M, Hosking LJ, Sandford RJ, Thomas HR (2020) A coupled compressible flow and geomechanics model for dynamic fracture aperture during carbon sequestration in coal. *Int J Numer Anal Methods Geomech* 44:1727–1749
- Cheng AH-D (2016) *Poroelasticity*. Springer, New York
- Choo J, White JA, Borja RI (2016) Hydromechanical modeling of unsaturated flow in double porosity media. *Int J Geomech*. [https://doi.org/10.1061/\(ASCE\)GM.1943-5622.0000558](https://doi.org/10.1061/(ASCE)GM.1943-5622.0000558)
- Choo J, Borja RI (2015) Stabilized mixed finite elements for deformable porous media with double porosity. *Comput Methods Appl Mech Eng* 293:131–154
- Coussy O (2004) *Poromechanics*. Wiley, Hoboken
- Deb R, Jenny P (2020) An extended finite volume method and fixed-stress approach for modeling fluid injection-induced tensile opening in fractured reservoirs. *Int J Numer Anal Methods Geomech* 44:1128–1144
- Gao Q, Ghassemi A (2020) Finite element simulations of 3D planar hydraulic fracture propagation using a coupled hydro-mechanical interface element. *Int J Numer Anal Methods Geomech* 44:1999–2024

23. Garipov TT, Karimi-Fard M, Tchelepi HA (2016) Discrete fracture model for coupled flow and geomechanics. *Comput Geosci* 20:149–160
24. Ge J, Jerath S, Ghassemi A (2020) Semianalytical modeling on 3D stress redistribution during hydraulic fracturing stimulation and its effects on natural fracture reactivation. *Int J Numer Anal Methods Geomech* 44:1184–1199
25. Ghafouri HR, Lewis RW (1996) A finite element double porosity model for heterogeneous deformable porous media. *Int J Numer Anal Methods Geomech* 20:831–844
26. Hajiabadi MR, Khoei AR (2019) A bridge between dual porosity and multiscale models of heterogeneous deformable porous media. *Int J Numer Anal Methods Geomech* 43:212–238
27. Jiang J, Younis RM (2016) Hybrid coupled discrete fracture/matrix and multicontinuum models for unconventional reservoir simulation. *SPE J* 21:1009–1027
28. Jin W, Arson C (2020) Fluid-driven transition from damage to fracture in anisotropic porous media: a multi-scale XFEM approach. *Acta Geotech* 15:113–144
29. Khalili N, Selvadurai APS (2003) A fully coupled constitutive model for thermo-hydro-mechanical analysis in elastic media with double porosity. *Geophys Res Lett* 30:1–5
30. Lemonnier P, Bourbiaux B (2010) Simulation of naturally fractured reservoirs. State of the art. Part 2 matrix-fracture transfers and typical features of numerical studies. *Oil Gas Sci Technol* 65:263–286
31. Lewallen KT, Wang HF (1998) Consolidation of a double-porosity medium. *Int J Solid Struct* 35:4845–4867
32. Lewis RW, Schrefler BA (1998) *The finite element method in the static and dynamic deformation and consolidation of porous media*. Wiley, Hoboken
33. Liu F (2020) Modeling hydraulic fracture propagation in permeable media with an embedded strong discontinuity approach. *Int J Numer Anal Methods Geomech* 44:1634–1655
34. Liu C, Prévost JH, Sukumar N (2019) Modeling branched and intersecting faults in reservoir-geomechanics models with the extended finite element method. *Int J Numer Anal Methods Geomech* 43:2075–2089
35. Ma J, Zhao G, Khalili N (2016) A fully coupled flow deformation model for elasto-plastic damage analysis in saturated fractured porous media. *Int J Plast* 76:29–50
36. Mehrabian A, Abousleiman YN (2014) Generalized Biot's theory and mandel's problem of multiple-porosity and multiple-permeability poroelasticity. *J Geophys Res Solid Earth* 119:2745–2763
37. Nguyen VX, Abousleiman YN (2010) Poroelastic solutions to plane strain and axisymmetric mandel-type problems in dual-porosity and dual-permeability medium. *J Appl Mech* 77:1–18
38. Niandou H, Shao JF, Henry JP, Fourmaintraux D (1997) Laboratory investigation of the mechanical behaviour of tournemire shale. *Int J Rock Mech Min Sci* 34:3–16
39. Nur A, Byerlee JD (1971) An exact effective stress law for elastic deformation of rock with fluids. *J Geophys Res* 76:6414–6419
40. Pergament A, Tomin P (2012) Single porosity model for fractured formations. In: *ECMOR XIII-13th European Conference on the Mathematics of Oil Recovery*
41. Pouragha M, Wan R, Eghbalian M (2019) Critical plane analysis for interpreting experimental results on anisotropic rocks. *Acta Geotech* 14:1215–1225
42. Ranjbar E, Hassanzadeh H (2011) Matrix fracture transfer shape factor for modeling flow of a compressible fluid in dual-porosity media. *Adv Water Resour* 34:627–639
43. Semnani SJ, White JA, Borja RI (2016) Thermo-plasticity and strain localization in transversely isotropic materials based on anisotropic critical state plasticity. *Int J Numer Anal Methods Geomech* 40:2423–2449
44. Shauer N, Duarte CA (2019) Improved algorithms for generalized finite element simulations of three-dimensional hydraulic fracture propagation. *Int J Numer Anal Methods Geomech* 43:2707–2742
45. Shiozawa S, Lee S, Wheeler MF (2019) The effect of stress boundary conditions on fluid-driven fracture propagation in porous media using a phase-field modeling approach. *Int J Numer Anal Methods Geomech* 43:1316–1340
46. Valliappan S, Khalili N (1990) Flow through fissured porous media with deformable matrix. *Int J Numer Methods Eng* 29:1079–1094
47. Vu MN, Pouya A, Seyedi DM (2014) Theoretical and numerical study of the steady-state flow through finite fractured porous media. *Int J Numer Anal Methods Geomech* 38:221–235
48. Tchelepi HA (2019) *Multiphase flow in porous media*, Stanford ENERGY 221 Lecture notes
49. Wang HF (2000) *Theory of linear poroelasticity with applications to geomechanics and hydrogeology*. Princeton University Press, New Jersey
50. Warren JE, Root PJ (1963) The behavior of naturally fractured reservoirs. *SPE J* 3:245–255
51. White JA, Castelletto N, Tchelepi HA (2016) Block-partitioned solvers for coupled poromechanics: a unified framework. *Comput Methods Appl Mech Eng* 303:55–74
52. Wilson RK, Aifantis EC (1982) On the theory of consolidation with double porosity. *Int J Eng Sci* 20:1009–1035
53. Wong T-F (2017) Anisotropic poroelasticity in a rock with cracks. *J Geophys Res Solid Earth* 122:7739–7753
54. Xu G, Gutierrez M, He C, Meng W (2020) Discrete element modeling of transversely isotropic rocks with non-continuous planar fabrics under Brazilian test. *Acta Geotech* 15:2277–2304
55. Zhang Q (2020) Hydromechanical modeling of solid deformation and fluid flow in the transversely isotropic fissured rocks. *Comput Geotech* 128:103812
56. Zhang Q, Choo J, Borja RI (2019) On the preferential flow patterns induced by transverse isotropy and non-Darcy flow in double porosity media. *Comput Methods Appl Mech Eng* 353:570–592
57. Zhao Y, Semnani SJ, Yin Q, Borja RI (2018) On the strength of transversely isotropic rocks. *Int J Numer Anal Methods Geomech* 42:1917–1934
58. Zhao Y, Borja RI (2020) A continuum framework for coupled solid deformation-fluid flow through anisotropic elastoplastic porous media. *Comput Methods Appl Mech Eng* 369:113225
59. Zheng H, Shi A-F, Liu Z-F, Wang X-H (2020) A dual-porosity model considering the displacement effect for incompressible two-phase flow. *Int J Numer Anal Methods Geomech* 44:691–704
60. Zhou S, Zhuang X (2020) Phase field modeling of hydraulic fracture propagation in transversely isotropic poroelastic media. *Acta Geotech* 15:2599–2618